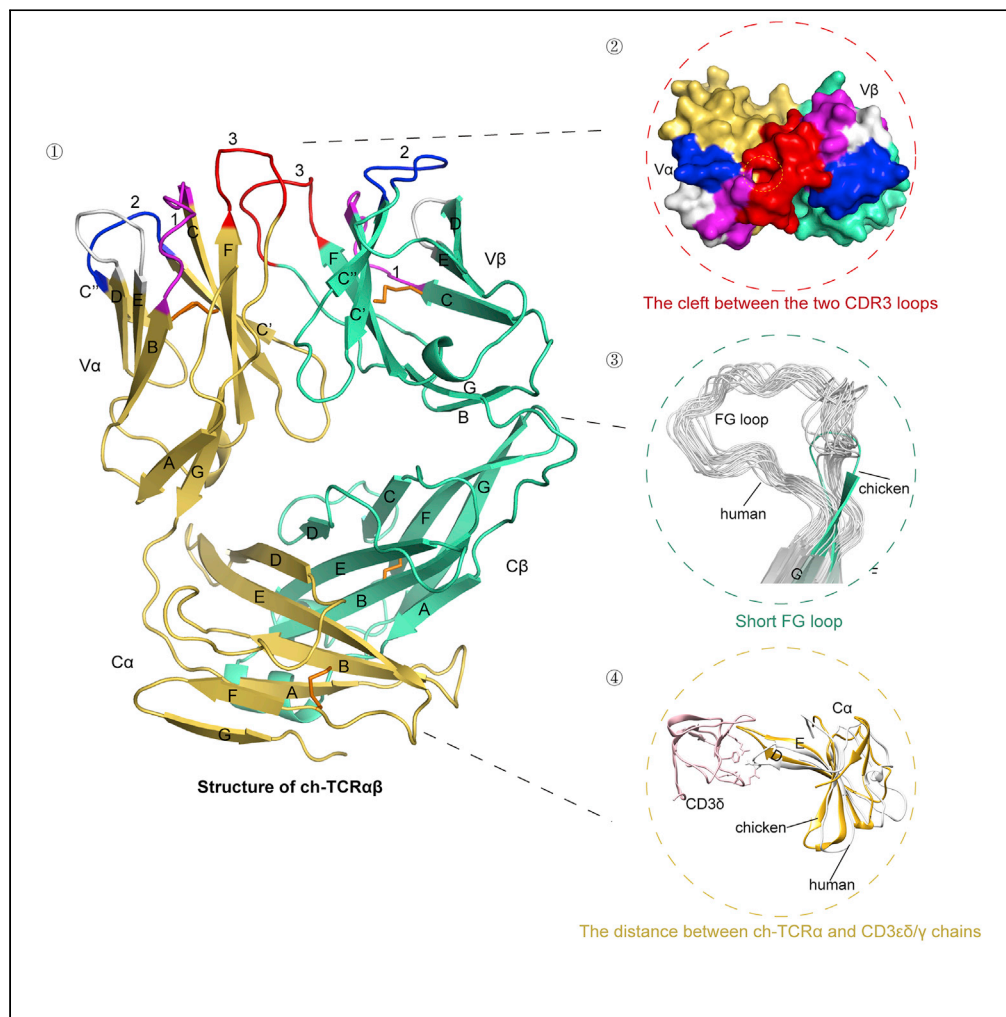


Article

Structural and Biophysical Insights into the TCR $\alpha\beta$ Complex in Chickens



Lijie Zhang, Yanjie Liu, Geng Meng, Ruiying Liang, Bing Zhang, Chun Xia

xiachun@cau.edu.cn

HIGHLIGHTS

Structural analysis of the overall architecture of the chicken TCR $\alpha\beta$ was completed

The positively charged cleft between the CDR3s might accommodate acidic side chains

The changes in the C domains of ch-TCR $\alpha\beta$ may impact the assembly of TCR-CD3 complex

The distinct topology of chicken TCR C β domain coevolved with CD3 heterodimers

Zhang et al., iScience 23, 101828
December 18, 2020 © 2020
The Author(s).
<https://doi.org/10.1016/j.isci.2020.101828>



Article

Structural and Biophysical Insights into the TCR $\alpha\beta$ Complex in ChickensLijie Zhang,^{1,2} Yanjie Liu,¹ Geng Meng,¹ Ruiying Liang,¹ Bing Zhang,¹ and Chun Xia^{1,3,*}

SUMMARY

In this work, chicken HPAIV H5N1 epitope-specific TCR $\alpha\beta$ (ch-TCR $\alpha\beta$) was isolated and its structure was determined. The C α domain of ch-TCR $\alpha\beta$ does not exhibit the typical structure of human TCR $\alpha\beta$, and the DE loop extends outward, resulting in close proximity between the C α domain of ch-TCR $\alpha\beta$ and CD3 $\epsilon\delta/\gamma$. The FG loop of the C β domain of ch-TCR $\alpha\beta$ is shorter. The changes in the C domains of ch-TCR $\alpha\beta$ and the difference in chicken CD3 $\epsilon\delta/\gamma$ confirm that the complexes formed by TCR $\alpha\beta$ and CD3 $\epsilon\delta/\gamma$ differ from those in humans. In the chicken complex, a positively charged cleft is formed between the two CDR3 loops that might accommodate the acidic side chains of the chicken pMHC-I-bound HPAIV epitope intermediate portion oriented toward ch-TCR $\alpha\beta$. This is the first reported structure of chicken TCR $\alpha\beta$, and it provides a structural model of the ancestral TCR system in the immune synapses between T cells and antigen-presenting cells in lower vertebrates.

INTRODUCTION

Specific T cell and antibody immunities are the two main lines of defense against viral, bacterial, and parasitic infections in jawed vertebrates. T cells recognize the antigenic peptides of these pathogenic microorganisms presented by major histocompatibility complex (MHC)-I/II bound to the peptide (pMHC-I/II) on antigen-presenting cells (APCs) through T cell receptors (TCR) and then trigger a specific T cell immune response by a series of signaling events (Davis and Bjorkman, 1988; Kaufman, 2018; Rudolph et al., 2006). The key link is that TCR and pMHC-I/II, the related co-receptors CD3 and CD8/CD4, and other costimulatory receptors, complete the first activation event in the immune synapses (Adams et al., 2016; Li et al., 2013; Sibener et al., 2018; Taniuchi, 2018). TCRs are heterodimers on the T cell surface composed of α - and β - or γ - and δ -chains linked by disulfide bonds. Each TCR chain consists of variable and constant Ig-like domains, followed by a transmembrane domain and a short cytoplasmic tail (Fields et al., 1995; Garcia et al., 1996). In addition, TCR binds to pMHC-I/II through the complementary-determining region (CDR) in its variable domain. To date, the complete TCR $\alpha\beta$ structure (Garcia et al., 1996; Kjer-Nielsen et al., 2002), TCR $\alpha\beta$ /pMHC complex (Reinherz et al., 1999; Stewart-Jones et al., 2003; Tynan et al., 2005), and TCR $\alpha\beta$ -CD3 complex from mammals have revealed a variety of ways for TCR to specifically recognize antigens (Dong et al., 2019). However, how these central immune protein molecules interact in the immune synapses has not been fully clarified by structural biology, and only some reasonable inferences are available (Li et al., 2013). It is worth noting that although these structures of pMHC-I, pMHC-II, and CD3 in nonmammals have been solved (Berry et al., 2014; Chen et al., 2017; Koch et al., 2007; Wu et al., 2017; Zhang et al., 2020a), the structure of TCR is still unknown. This lack of information particularly hinders the understanding of immunology in lower vertebrates.

A series of achievements have been made in the study of chicken TCR. Chicken TCR studies began with the demonstration of the TCR-CD3 complex on the surface of chicken T cells by using monoclonal antibodies (Chen et al., 1986). Subsequently, three TCRs (TCR1, TCR2, and TCR3) were identified and found to be successively expressed during the development of chicken T cells (Chen et al., 1989; Lahti et al., 1988). Chicken TCR1 is TCR $\gamma\delta$, and both TCR2 and TCR3 are TCR $\alpha\beta$. The α chains of chicken TCR2 and TCR3 are identical, but the variable regions in the β chain are different and are encoded by the V β 1 and V β 2 genes, respectively (Tjoelker et al., 1990). Each of the chicken TCR chains is encoded by a separate combination of genes (Cooper et al., 1991; Shigeta et al., 2004; Tjoelker et al., 1990). For example, the chicken α chain is encoded by TCR-V genes, TCR-J genes, and TCR-C genes, whereas β chains are encoded by these three genes as well as by various TCR-D genes. In addition, the chicken TCR β gene locus is very simple compared with that of mammals; it contains only two major V β gene families (V β 1 and V β 2) and one D-J-C gene cluster that includes one D gene, four J genes, and one C gene (Shigeta et al., 2004). The main chicken TCR α gene

¹Department of Microbiology and Immunology, College of Veterinary Medicine, China Agricultural University, Haidian District, Beijing 100193, China

²Joint National Laboratory for Antibody Drug Engineering, Key Laboratory of Cell and Molecular Immunology, School of Medical Sciences, Henan University, Kaifeng 475004, China

³Lead contact

*Correspondence: xiachun@cau.edu.cn

<https://doi.org/10.1016/j.isci.2020.101828>



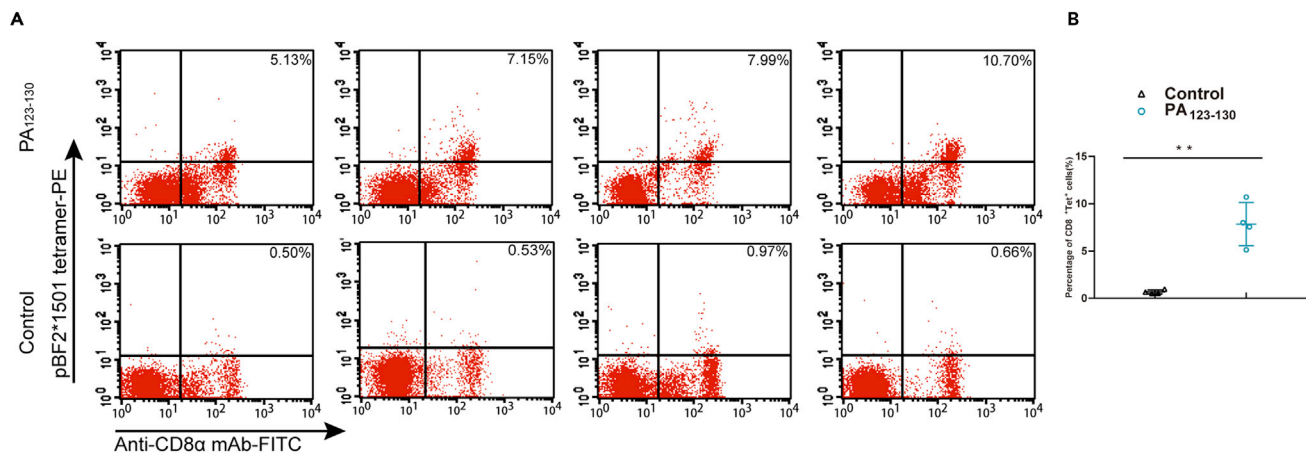


Figure 1. Detection of CD8⁺ Tet⁺ T Cells from Immunized and Control B15 Chickens

(A and B) (A) Peripheral blood mononuclear cells (PBMCs) were isolated from each of 12 chickens (4 chickens in each group) and stained with both the PE-labeled pBF2*15:01 tetramer (Tet) that incorporated the peptide PA₁₂₃₋₁₃₀ and an fluorescein isothiocyanate-labeled anti-CD8 monoclonal antibody. Flow cytometry was performed to detect CD8⁺ T cells that were specific for the peptide PA₁₂₃₋₁₃₀ (i.e., CD8⁺ Tet⁺ T cells). The data are presented as pseudocolor plots. The percentage of cells in the tetramer and CD8 double-positive areas was 5.13%–10.70% for the peptide-immunized animals. The cells in the double-positive areas of the control group were scattered and nonspecific, accounting for 0.50%–0.97% of the total cells. (B) Statistical analysis confirmed that the percentages of PA₁₂₃₋₁₃₀ epitope-specific CD8⁺ T cells were significantly higher in the peptide-immunized group than in the control group ($p < 0.01$). The data are shown as the mean \pm SEM. ** $p < 0.01$ by unpaired t test.

region includes the V α 1 family (41 genes), the V α 2 family (19 genes), 48 J α genes, and one C α gene (Chen et al., 1996; Kubota et al., 1999; Parra and Miller, 2012). Surprisingly, chickens lack distinct CD3 γ and CD3 δ subunits but express a hybrid CD3 δ/γ protein that shares equal homology with mammalian CD3 δ and CD3 γ (Gobel and Dangy, 2000). The chicken CD3 $\epsilon\delta/\gamma$ molecule displays significant differences from the human and mouse CD3 molecules in both its packing orientation and its dimer interface (Berry et al., 2014). During chicken T cell activation and signaling, the key molecules pMHC-I/II, CD8, and CD3 have been known. However, knowledge of the other key molecules TCR $\alpha\beta$ and pMHC-I/II is still lacking, and this prevents us from achieving a deep and systematic understanding of chicken immunology.

In this study, the crystal structure of chicken TCR $\alpha\beta$ (ch-TCR $\alpha\beta$) was determined. The C α domain of ch-TCR $\alpha\beta$ does not exhibit the structure typical of human TCR $\alpha\beta$. The extension of the DE loop of the C α domain, the shortening of the FG loop of the C β domain, and the difference in the packing orientation of CD3 $\epsilon\delta/\gamma$ confirm that the complexes formed by chicken TCR $\alpha\beta$ (ch-TCR $\alpha\beta$) and CD3 $\epsilon\delta/\gamma$ are very different from those of humans. In ch-TCR $\alpha\beta$, there is a positively charged cleft between the two CDR3 loops that might accommodate the acidic side chains of the MHC-bound peptide intermediate portion oriented toward ch-TCR $\alpha\beta$. These results provide key guidance for TCR-based T cell recognition, and provide key knowledge of the molecular anatomy between T cells and APC in the immune synapses of chickens.

RESULTS

Epitope-Specific TCR $\alpha\beta$ Genes in CD8⁺ T Cells

Tetrameric pBF2*1501 complexes constructed for the PA₁₂₃₋₁₃₀ peptide are shown in Figure S1. After immunizing B15-haplotype chickens with PA₁₂₃₋₁₃₀ peptide, flow cytometry analysis showed that the percentage of CD8⁺ T cells specific to the PA₁₂₃₋₁₃₀ peptide was significantly greater in the immunized group than in the control group (Figure 1). The percentage of CD8⁺ double-positive T cells was 5.13%–10.70% in the peptide-immunized group and 0.50%–0.97% in the control group (Figure 1A). Statistical analysis confirmed that there was a very significant difference between the group immunized with the PA₁₂₃₋₁₃₀ peptide and the control group ($p < 0.01$). As the percentage of double-positive T cells in the immunized group was significantly higher than that in the control group, the PA₁₂₃₋₁₃₀ epitope-specific CD8⁺ T cells were easily sorted by flow cytometry (Li et al., 2020). The TCR α/β genes and amino acid sequences derived from PA₁₂₃₋₁₃₀ epitope-specific CD8⁺ T cells have been submitted to GenBank (GenBank: MN646854 and MN646855). The ch-TCR α gene is 810 bp in length and encodes a protein of 269 amino acids. The cloned ch-TCR α consists of the V α 1.4 segment of the V α 1 family, a J α segment and the only C α segment. The cloned ch-TCR β gene is 852 bp in length and encodes a protein of 283 amino acids. The

chicken *TCR β* gene locus is very simple compared with that of mammals. According to the genomic organization of the chicken *TCR β* locus, *ch-TCR β* is composed of the V β 2.2 segment, the J β 3 segment, the D β segment, and the C β segment (Zhang et al., 2020b).

The Architecture of ch-TCR $\alpha\beta$

The extracellular regions of the ch-TCR α and ch-TCR β genes were subcloned for prokaryotic expression (Table S1). Ch-TCR α and ch-TCR β formed a heterodimer *in vitro* (Figure S2). The high-purity ch-TCR $\alpha\beta$ was used to screen crystals; this led to the collection of a set of diffraction data at a resolution of 2.1 Å for ch-TCR. However, in the process of structural determination, only the solution of the ch-TCR α chain can be solved, and the solution of the ch-TCR β chain cannot be obtained by the available methods. Therefore, we performed amino acid mutagenesis of the ch-TCR β chain, introduced selenomethionine, and collected the diffraction data at a resolution of 1.9 Å for selenomethionine (SeMet)-ch-TCR $\alpha\beta$. The crystal structure of ch-TCR $\alpha\beta$ was determined by a combination of molecular replacement and single-wavelength anomalous diffraction (SAD) phasing. The final refinement of the structure generated R/R_{free} factors of 0.205/0.236 (Table 1). Crystal structure analysis of ch-TCR $\alpha\beta$ showed two molecules in each asymmetric unit (Figure S3). The two molecules were very similar (Figure S3). Apart from certain key features, the topology of the ch-TCR $\alpha\beta$ structure is basically the same as that of known TCR $\alpha\beta$ structures (Figure 2).

Multiple sequence alignment showed that ch-TCR α shares less than 35% amino acid sequence identity with human and mouse TCR α (Figure 3). The similarity of the C α domain was less than 23%, whereas the similarity of the ABED sheet was between 22% and 24%, and the similarity of the CFG sheet was no more than 18%; in particular, the similarity with the C α chain of 2C (PDB: 1TCR) was only 7% (Figure 3). The similarity between the β chains was 35%–46%, higher than that of the α chains. The similarity between C β domains was higher than 40%, but there was a large fragment deletion between the F and G strands. The difference in amino acid sequences may indicate that ch-TCR $\alpha\beta$ has certain species-specific characteristics.

ch-TCR $\alpha\beta$ Structure Reveals a Close Connection with the CD3 Molecule

Superposition of the ch-TCR $\alpha\beta$ structure and the solved TCR $\alpha\beta$ structures showed the greatest difference in the C α domain, where the root-mean-square deviation of the α -carbon positions was greater than 2.0 Å (Table S2). The C α domain of ch-TCR $\alpha\beta$ showed lower thermal factors (B values) than in the other resolved TCR $\alpha\beta$ structures. The most obvious difference between the C α domain of ch-TCR $\alpha\beta$ and that of previously solved TCR $\alpha\beta$ structures was in the CFG sheet (Figure 4A). The CFG sheet of the C α domain consisted of a regular IgSF-C1 domain. Hydrogen bonds between the main chains of the C, F, and G strands maintained the standard CFG sheet conformation (Figure 4B). The C α domains of human and mouse TCR $\alpha\beta$ contain unusual secondary structures that are highly divergent from the standard IgSF-fold (Figure 4C). Additionally, the F segment in human and mouse TCR $\alpha\beta$ formed an unusual one-turn mini-helix that lacked hydrogen bonds to the neighboring strands (Figure 4D). There was no mini-helix in the C α domain of ch-TCR $\alpha\beta$, and the position that the mini-helix would have occupied instead contained the regular F strand (Figure 4A). The C α domain of ch-TCR $\alpha\beta$ was identical to that of the previously solved TCR $\alpha\beta$; the two sheets were far apart, and the connection was looser than that of the classic IgSF-C1-fold (Figure S4). It is worth mentioning that the C δ domain of TCR $\gamma\delta$ also retained the classical IgSF-fold similar to that of ch-TCR $\alpha\beta$. These characteristics indicate that the C α domain of ch-TCR $\alpha\beta$ adopts a conformation intermediate between that of human and mouse TCR $\alpha\beta$ and classical IgSF-C1.

The ABED sheet was similar to the corresponding sheet in IgSF-C1 domains and other TCR $\alpha\beta$ structures, but there were also some differences, mainly in the region between the D and E strands (Figure 4E). Compared with those of previously reported TCR $\alpha\beta$ structures, the D and E strands of ch-TCR $\alpha\beta$ were longer. The direction of the DE loop between the D and E strands changed, and the loop extended farther outward, playing a key role in binding to the CD3 molecule. At certain matching positions in the DE loop, the distance between the superposed ch-TCR $\alpha\beta$ and human TCR-CD3 complex structures was very short, even constituting close contact (Figure 4F). Because chicken CD3 $\epsilon\delta/\gamma$ has a unique packing orientation and dimer interface compared with mammalian CD3 $\epsilon\gamma$ and CD3 $\epsilon\delta$, ch-TCR $\alpha\beta$ and ch-CD3 may enable the formation of a signaling complex that differs from the complex found in humans. Amino acid sequence alignment showed that the deletion of amino acids 148–152 and the insertion of amino acids 159–162 in ch-TCR $\alpha\beta$ might have caused the shift in the DE loop. Apart from a few amino acid substitutions, the C α domains of TCR $\alpha\beta$ were conserved in chickens. This feature was common in chickens and is considered a species characteristic.

	ch-TCR	SeMet ch-TCR
Data collection		
Space group	P1211	P 1 21 1
Cell dimensions		
a, b, c (Å)	77.43, 83.097, 82.416	76.48, 77.40, 80.60
α, β, γ (°)	90, 117.716, 90	90.00, 116.02, 90.00
Wavelength (Å)	0.97923	0.97923
Absorption (Se)		Peak
Resolution (Å)	29.29–2.091 (2.166–2.091) ^a	77.40–2.1 (2.15–2.10)
Total reflections	382,365	378,197
Unique reflections	54,200	49,681
Rsym or Rmerge ^b	0.114(0.860) ^a	0.092(0.646)
$I/\sigma I$	15.1(3.5) ^a	14.9(3.3)
Completeness (%)	99.4 (97) ^a	99.9 (99.9) ^a
Redundancy	7.1(5.6)	7.6 (7.7)
Refinement		
No. Reflections	52,142	
R_{work}/R_{free} (%) ^c	20.5/23.6	
RMS deviations		
Bond lengths (Å)	0.02	
Bond angles (°)	1.97	
Average B factor	50.16	
Ramachandran plot quality		
Most favored region (%)	94.91	
Allowed region (%)	5.08	
Disallowed (%)	0.00	

Table 1. Data Collection and Refinement Statistics

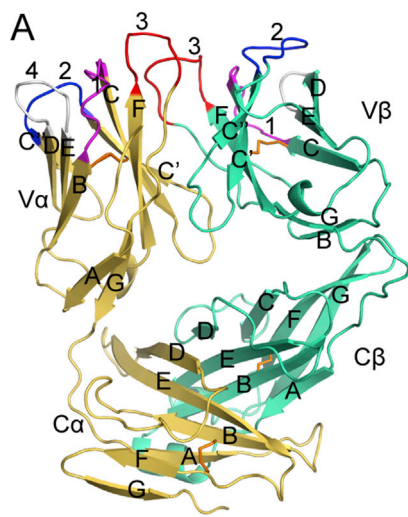
^aValues in parentheses represent the highest resolution shell.

^b $R_{merge} = \sum_i \sum_{hkl} |I_i(hkl) - \langle I(hkl) \rangle| / \sum_i \sum_{hkl} I_i(hkl)$, where $I_i(hkl)$ is the observed intensity and $\langle I(hkl) \rangle$ is the average intensity recorded in multiple measurements.

^c $R = \sum_{hkl} ||F_{obs} - k|F_{calc}|| / \sum_{hkl} |F_{obs}|$, where Rfree is calculated for a randomly chosen 5% of reflections and R_{work} is calculated for the remaining 95% of reflections used for structure refinement.

Short FG Loop of the C β Domain in ch-TCR $\alpha\beta$ Caused by 12-Residue Deletion

Superposition of ch-TCR $\alpha\beta$ with the previously solved TCR $\alpha\beta$ structures revealed that there were also large differences in the C β domain (Figure 5A). First, the FG loop of the C β domain of ch-TCR $\alpha\beta$ was shorter (Figures 5A and 5B). The C β domains of mice and humans contain an elongated 12-residue FG loop that extends out to the side of the C β domain and adopts a roughly similar conformation in the two species. Sequence alignment of the FG loop regions of the C β domains of various species showed that whereas the 12-residue insertion is well conserved among mammals, nonmammals do not have this 12-residue insertion within the FG loop (Figure 5C). In $\alpha\beta$ T cells, the FG loop is important for development, thymic selection, and T cell function and has recently been shown to be important for sustained TCR-MHC binding and T cell signaling (Brazin et al., 2015; Wang, 2020). It has also been suggested to be important for CD3 ϵ binding. The unique structure of the ch-CD3 molecule suggests that ch-TCR $\alpha\beta$ with a short FG loop may

**Figure 2. Cartoon Representation of ch-TCR $\alpha\beta$**

The four pairs of disulfide bonds are represented by orange sticks within each domain. The β strands are labeled according to the solved TCR $\alpha\beta$ structures. The CDR1 loops of ch-TCR $\alpha\beta$ are displayed in magenta, and the CDR2 loops are displayed in blue. The CDR3 loops are colored red, and HV4 are shown in gray.

bind ch-CD3 in different ways, and ch-TCR $\alpha\beta$ may have different signaling mechanisms. In fact, the insertion of 12 residues occurs only in the C γ domain of TCR $\gamma\delta$ and in the mammalian C β domain of TCR but not in other IgSF structures.

Interactions within the ch-TCR $\alpha\beta$ Heterodimer

Although the conformation of the C regions was significantly altered, it remained relatively conserved at the interface between C α and C β . The C α -C β interface was highly polar, with a skewed distribution of acidic residues on the C α domain and basic residues on the C β domain and the presence of many other polar residues, and included hydrogen bond interactions between polar residues on the C α domain and charged residues on the C β domain, or vice versa (Figure 5D). The C α -C β interface was stabilized by many hydrogen bonds and van der Waals interactions. Because there is no long FG loop, the buried area between C β -V β is small. The binding angle between the C β and V β domains was similar to that of the resolved TCR $\alpha\beta$ structures. Because the F and G strands of the C β domain of ch-TCR $\alpha\beta$ were longer than those in the other TCR $\alpha\beta$ structures and the N terminus of the G strand was closer to the V β domain, two hydrogen bonds formed between β 211Gln and β 6Ser/ β 7Ile, but no other hydrogen bonds existed. There was no hydrogen bond at the V α -C α interface, and the angle and stability of the elbow region were maintained mainly by van der Waals interactions.

Conformation of the CDR Loops of ch-TCR $\alpha\beta$

The CDR loops in the ch-TCR $\alpha\beta$ structure were labeled and analyzed according to the accepted division of CDRs and the solved human TCR $\alpha\beta$ structures (Figures 6A and 6B). The CDR1s and CDR2s of ch-TCR $\alpha\beta$ were relatively invariant germline genetic coding components that were derived directly from different variable region gene segments (Figure 6C); the CDR3s of ch-TCR $\alpha\beta$ were highly variable components obtained by the random addition and deletion of nucleotides during gene rearrangement and by the random combination of numerous linker gene fragments and the variable gene fragments V/(D)/J (Figure 3).

The CDR1 β loop of ch-TCR β was stabilized predominantly by hydrogen bonds between β 22Gln, β 26His, and β 27Asp located on the CDR1 β loop and residues located on the HV4 β and CDR3 β loops (Figure 6D). The CDR2 β loop of ch-TCR β linked the C' and C'' strands, which were the edge strands of two sheets. The CDR2 β loop of ch-TCR β was stabilized by intraloop hydrogen bonds. β 65Arg and the residues of the CDR1 β and CDR2 β loops of ch-TCR β formed a network of five hydrogen bonds that played an important role in maintaining the stability of the CDR1 β and CDR2 β loops. The CDR1 α loop of ch-TCR α was stabilized by hydrogen bonds formed by the backbone atoms of the residues located in the CDR1 α loop and the side chains of the residues located in the CDR3 α and HV4 loops. The CDR2 α loop of ch-TCR α consisted of five residues with no intraloop interaction. There was only a hydrogen bond between the two CDR3 loops of ch-TCR $\alpha\beta$, so that the two CDR3s loops tended to face each other (Figure 6E). The CDR loops of TCR $\alpha\beta$ are highly flexible, and these analyses only represent the conformations in that structure. The buried surface

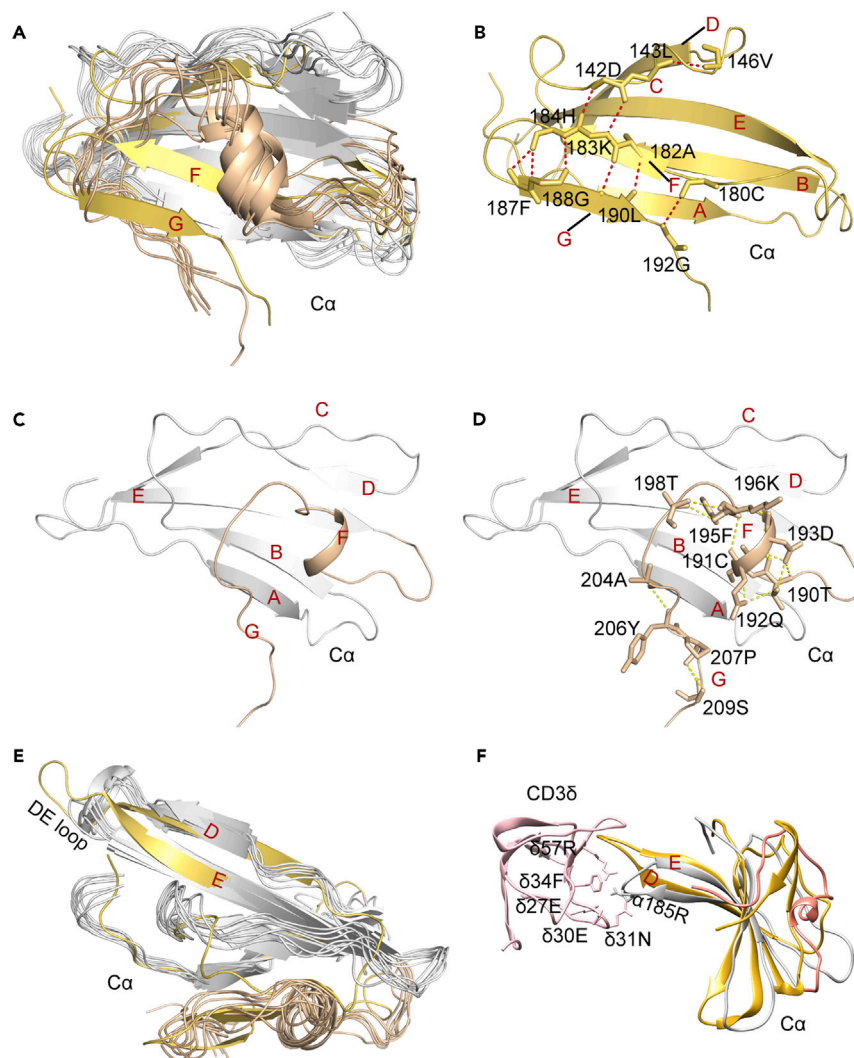


Figure 4. Structural Analysis of the Differences between the C α Domain of Chicken TCR $\alpha\beta$ and that of Human and Mouse TCR $\alpha\beta$

(A) Superposition of the C α domain of ch-TCR $\alpha\beta$ with the human and mouse TCR $\alpha\beta$ structures. The most obvious difference between the ch-TCR $\alpha\beta$ and previously solved TCR $\alpha\beta$ structures is the CFG sheet. The C α domain of ch-TCR $\alpha\beta$ is shown in yellow-orange. The ABED sheet of other resolved TCR $\alpha\beta$ molecules are shown in gray, and the CFG sheet is shown in light pink.

(B) Detailed analysis of the hydrogen bonds between the main chains of the CFG sheet of ch-TCR $\alpha\beta$. The amino acids involved in the formation of hydrogen bonds are shown in stick representation, and the hydrogen bonds are shown as red dashed lines.

(C) Conformation of the C α domain of human and mouse TCR $\alpha\beta$ taking 2C-TCR $\alpha\beta$ (PDB: 1TCR) for example.

(D) Detailed analysis of the hydrogen bonds between the main chains of the CFG sheet region of 2C-TCR $\alpha\beta$.

(E) Compared with those in the previously solved TCR $\alpha\beta$ structure, the D and E strands of ch-TCR $\alpha\beta$ are longer. The DE loop between the D and E strands of ch-TCR $\alpha\beta$ also differs; its direction differs from that of the DE loop in the other structures, and it extends further outward.

(F) The difference in the DE loop led to variation in CD3 $\epsilon\delta$ binding. When the chicken CD3 δ/γ chain was superposed with the human CD3 δ chain, the distance between the superposed ch-TCR α chain and the CD3 $\epsilon\delta/\gamma$ chain is very short, even indicating close contact. CD3 δ is shown in pink.

and CDR2 β loops of TCR recognize and bind to the α 1 helix of MHC-I. Asp and Tyr at positions 27 and 28 of ch-TCR β and Tyr at position 47 of ch-TCR β potentially bind to the MHC-I α 1 helix. β 47Tyr was conserved in most species and was positioned over a similar site on the MHC-I α 1 helix. The CDR1 α and CDR2 α loops of TCR recognize and bind to the α 2 helix of MHC-I. Tyr at position 28 and Val and Lys at positions 48 and 49 of

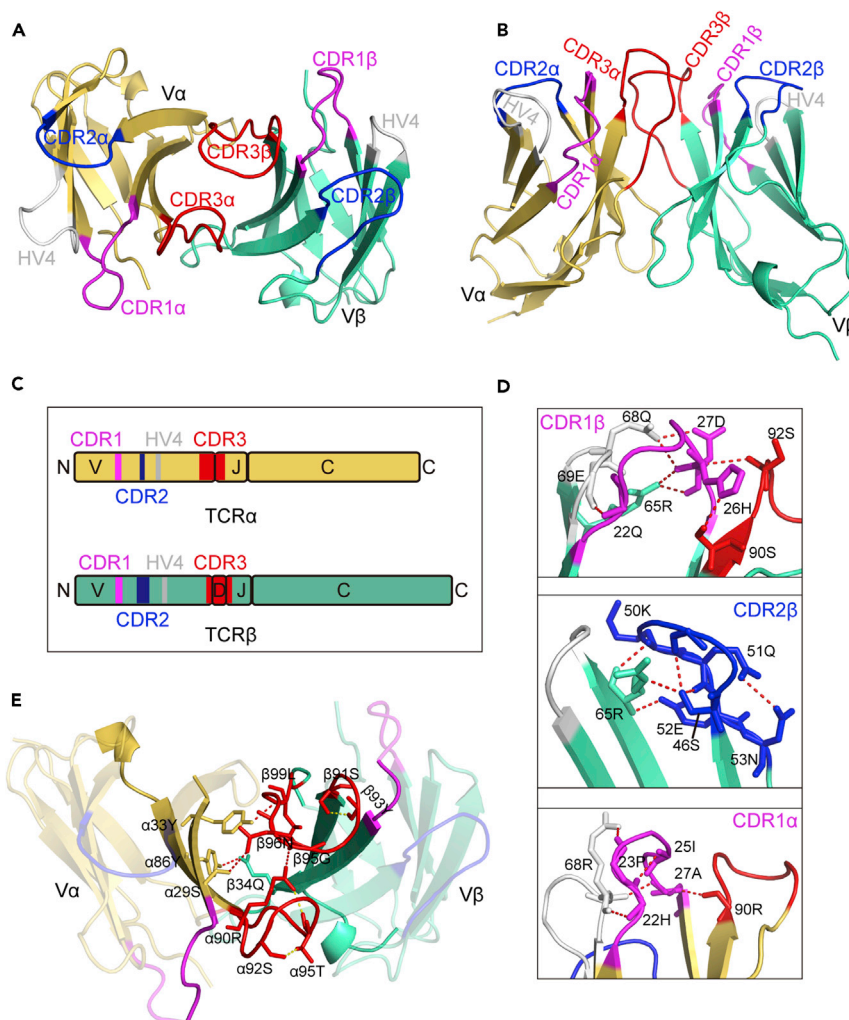


Figure 6. Conformation of the CDR Loops of ch-TCR $\alpha\beta$

(A) Top view of the CDR loops. The color of the CDR loops of ch-TCR $\alpha\beta$ is as in Figure 2.

(B) Side view of the CDR loops.

(C) Schematic representation of the gene fragments encoding the chicken TCR α chain and the chicken TCR β chain. Each of the TCR chains is encoded by a combination of separate genes. The α chains are encoded by TCR-V genes, TCR-J genes, and TCR-C genes, whereas the β chains are encoded by these three genes plus variable TCR-D genes. The CDR1 and CDR2 loops are encoded within the V genes. CDR3 occurs at the V-J junction in the α chain and at the V-D-J junction in the β chain.

(D) From top to bottom, detailed analysis of the interactions that maintain the conformations of the CDR1 β , CDR2 β , and CDR1 α loops.

(E) Analysis of the interactions between the variable domains. The sites of interaction between the V α and V β domains are indicated by red dashes. The internal interactions of the CDR3 α and CDR3 β loops are indicated by yellow dashes.

outward and plays a key role in binding to the CD3 molecule. Another interesting feature is that the FG loop of the C β domain of ch-TCR $\alpha\beta$ is shorter (Figure 4). In the mouse and human C β domains, the elongated 12-residue FG loop extends out to the side of the domain (Wang and Reinherz, 2012). The FG loop is important for development, thymic selection, and T cell function and has recently been shown to be important for sustained TCR-MHC binding during TCR-pMHC interactions and T cell signaling (Brazin et al., 2015).

The immune synapses in which a specific TCR interacts with pMHC-I/II are formed on the surface of T cells and APC; within the synapse, the V region of TCR recognizes the peptide and the binding region of pMHC-I/II and receives important signals in T cell activation (La Gruta et al., 2018). Subsequently, the C region, the

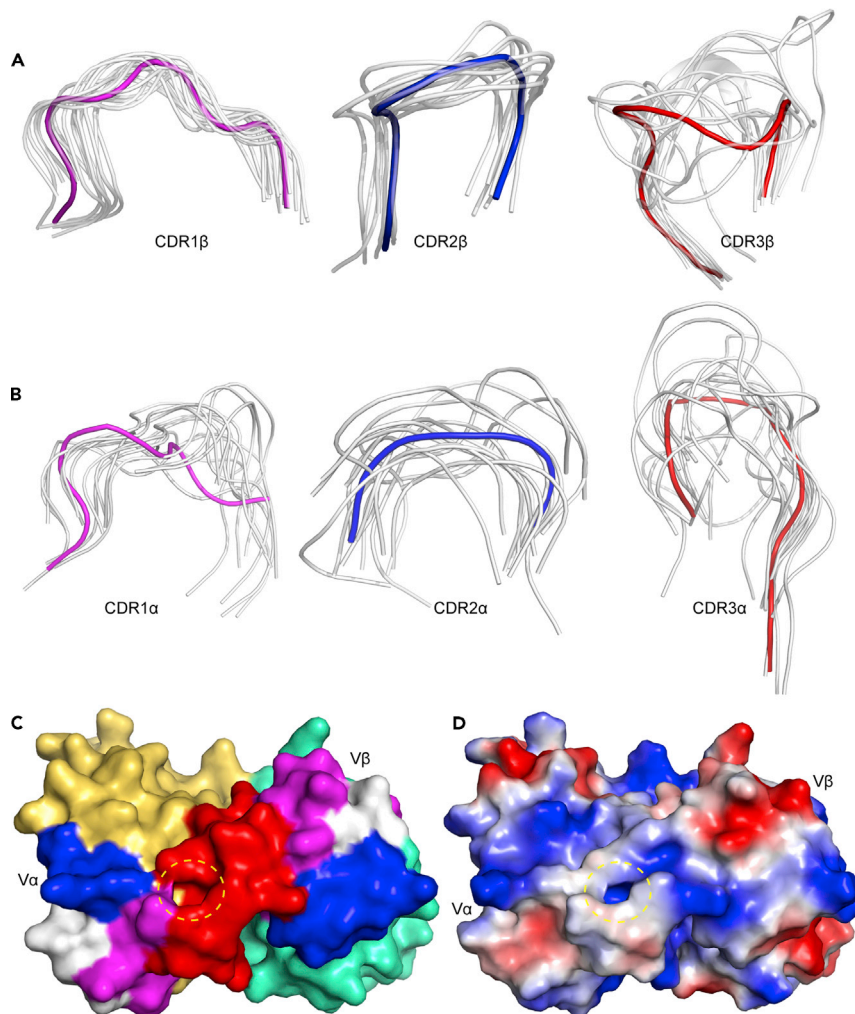


Figure 7. Structural Analysis of the CDR Loops of ch-TCR $\alpha\beta$

(A) Top view of the CDR loops shown on the surface.

(B) Top view of the CDR loops shown as polarity. Red indicates negative polarity, and blue indicates positive polarity.

(C and D) The CDR1, CDR2, and CDR3 loops of the α and β chains were analyzed and compared in detail. The color of the CDR loops of ch-TCR $\alpha\beta$ is as in Figure 2. The CDR loops of other resolved TCR $\alpha\beta$ structures are shown in gray.

transmembrane region, and the intracellular region of the TCR bind to the CD3 molecule and transmit the signal downstream (Dong et al., 2019). Based on the structure of the human TCR-CD3 complex (Dong et al., 2019), it was found that when the chicken δ/γ chain was superposed with the human δ chain, the ch-TCR α chain was oriented toward CD3 $\epsilon\delta/\gamma$ and the distance between the superposed ch-TCR α chain and the CD3 $\epsilon\delta/\gamma$ chain was very small, even suggesting overlap; this was not a reasonable combination. When the ϵ chains of chicken and human were superimposed, the distance between the ch-TCR α chain and the CD3 δ/γ chain was reasonable, but the binding surface differed from that of the TCR-CD3 complex in humans. It is also possible that the CD3 ϵ and CD3 δ/γ chains of chicken do not function in the same manner as the human ϵ and δ chains but are instead employed in a completely novel way. There are elongated FG loops in the TCR C β domains and separately expressed CD3 δ and γ chains in mammals, whereas short FG loops and hybrid CD3 δ/γ chains are common in nonmammals; this indicates that the distinct topology of CD3 heterodimers coevolved with TCR C β domains to optimize the quaternary TCR structure for pMHC-I/II-triggered TCR activation (Brazin et al., 2015; Kim et al., 2010). Therefore, it is certain that the combination of chicken TCR $\alpha\beta$ and CD3 $\epsilon\delta/\gamma$ differs from that of humans. The more highly conserved chicken $\zeta\zeta$ chain can replace its mouse counterpart in $\zeta\zeta$ -deficient T cells and send signals downstream (Gobel and Bolliger, 1998). Assembly of the TCR-CD3 complex is mediated by its ECDs, CPs, and transmembrane helices. The CP and transmembrane interactions play a major role in the assembly

of the TCR-CD3 complex, whereas the ECD interactions are secondary (Call et al., 2002). The correct binding conformation between ch-TCR and ch-CD3 molecules has not yet been determined, and the structure of the complex must be resolved to clarify its actual conformation.

When interacting with MHC molecules, the greatest difference observed was that the two CDR3s of ch-TCR $\alpha\beta$ were bound by only a single hydrogen bond between the two loops; thus the two CDR3s tended to face each other. In ch-TCR $\alpha\beta$, a positively charged cleft that might accommodate the side chains of acidic residues of PA₁₂₃₋₁₃₀ was formed between the two CDR3 loops (Figures 6C and 6D, Figure 7). Detailed interaction residues and docking angles between pMHCII and ch-TCR $\alpha\beta$ require structural data to be obtained.

Limitations of the Study

In this study, we provided a detailed structural analysis of the overall architecture of the chicken TCR $\alpha\beta$ that served as a molecular basis for a comparative investigation with other TCR $\alpha\beta$ structures from other distant species, and in the context of the immune synapse. Here, the study showed that the DE and FG loop in the chicken TCR $\alpha\beta$ were longer and shorter, respectively, than the mammalian counterparts, suggesting that it may impact in overall assembly of the chicken immune synapse. However, if we can obtain the chicken TCR-MHC structure further, this will greatly strengthen the article immensely.

Resource Availability

Lead Contact

All relevant data and requests for resources and reagents should be directed to and will be fulfilled by the Lead Contact, Chun Xia (xiachun@cau.edu.cn).

Materials Availability

This study did not generate new unique reagents.

Data and Code Availability

The coordinates and structure factors generated in this study have been deposited to the Protein DataBank under accession number 6LIR.

METHODS

All methods can be found in the accompanying [Transparent Methods supplemental file](#).

SUPPLEMENTAL INFORMATION

Supplemental Information can be found online at <https://doi.org/10.1016/j.isci.2020.101828>.

ACKNOWLEDGMENTS

This work was supported by the National Natural Science Foundation of China (grants 31972683 and 31572493). We thank Professor Jianxun Qi (Institute of Microbiology, Chinese Academy of Sciences) for his help in structure refinement. We acknowledge the assistance of the staff at the Shanghai Synchrotron Radiation Facility of China.

AUTHOR CONTRIBUTIONS

C.X. designed the study and supervised the project; L.Z., Y.L., R.L., and B.Z. performed experiments; L.Z. performed the data analysis; L.Z. and G.M. solved the structure; C.X. provided guidance on data analysis; C.X. and L.Z. wrote the paper.

DECLARATION OF INTEREST

The authors declare no competing interest.

Received: July 9, 2020

Revised: September 16, 2020

Accepted: November 16, 2020

Published: December 18, 2020

REFERENCES

- Adams, J.J., Narayanan, S., Birnbaum, M.E., Sidhu, S.S., Blevins, S.J., Gee, M.H., Sibener, L.V., Baker, B.M., Kranz, D.M., and Garcia, K.C. (2016). Structural interplay between germline interactions and adaptive recognition determines the bandwidth of TCR-peptide-MHC cross-reactivity. *Nat. Immunol.* **17**, 87.
- Berry, R., Headey, S.J., Call, M.J., McCluskey, J., Tregaskes, C.A., Kaufman, J., Koh, R., Scanlon, M.J., Call, M.E., and Rossjohn, J. (2014). Structure of the chicken CD3epsilon/delta/gamma heterodimer and its assembly with the alphabeta T cell receptor. *J. Biol. Chem.* **289**, 8240–8251.
- Brazin, K.N., Mallis, R.J., Das, D.K., Feng, Y., Hwang, W., Wang, J.H., Wagner, G., Lang, M.J., and Reinherz, E.L. (2015). Structural features of the alphabeta TCR mechanotransduction apparatus that promote pMHC discrimination. *Front. Immunol.* **6**, 441.
- Call, M.E., Pyrdol, J., Wiedmann, M., and Wucherpfennig, K.W. (2002). The organizing principle in the formation of the T cell receptor-CD3 complex. *Cell* **111**, 967–979.
- Chen, C.H., Six, A., Kubota, T., Tsuji, S., Kong, F.K., Gobel, T.W., and Cooper, M.D. (1996). T cell receptors and T cell development. *Curr. Top Microbiol. Immunol.* **212**, 37–53.
- Chen, C.H., Sowder, J.T., Lahti, J.M., Cihak, J., Losch, U., and Cooper, M.D. (1989). TCR3: a third T-cell receptor in the chicken. *Proc. Natl. Acad. Sci. U. S. A.* **86**, 2351–2355.
- Chen, C.L., Ager, L.L., Gartland, G.L., and Cooper, M.D. (1986). Identification of a T3/T cell receptor complex in chickens. *J. Exp. Med.* **164**, 375–380.
- Chen, Z., Zhang, N., Qi, J., Chen, R., Dijkstra, J.M., Li, X., Wang, Z., Wang, J., Wu, Y., and Xia, C. (2017). The structure of the MHC class I molecule of bony fishes provides insights into the conserved nature of the antigen-presenting system. *J. Immunol.* **199**, 3668–3678.
- Cooper, M.D., Chen, C.-L.H., Bucy, R.P., and Thompson, C.B. (1991). Avian T cell ontogeny. *Adv. Immunol.* **50**, 87–117.
- Davis, M.M., and Bjorkman, P.J. (1988). T-cell antigen receptor genes and T-cell recognition. *Nature* **334**, 395–402.
- Dong, Zheng, L., Lin, J., Zhang, B., Zhu, Y., Li, N., Xie, S., Wang, Y., Gao, N., and Huang, Z. (2019). Structural basis of assembly of the human T cell receptor-CD3 complex. *Nature* **573**, 546–552.
- Fields, B.A., Ober, B., Malchiodi, E.L., Lebedeva, M.I., Braden, B.C., Ysern, X., Kim, J.K., Shao, X., Ward, E.S., and Mariuzza, R.A. (1995). Crystal structure of the V alpha domain of a T cell antigen receptor. *Science* **270**, 1821–1824.
- Garcia, K.C., Degano, M., Stanfield, R.L., Brunmark, A., Jackson, M.R., Peterson, P.A., Teyton, L., and Wilson, I.A. (1996). An alphabeta T cell receptor structure at 2.5 Å and its orientation in the TCR-MHC complex. *Science* **274**, 209–219.
- Gobel, T.W., and Bolliger, L. (1998). The chicken TCR zeta-chain restores the function of a mouse T cell hybridoma. *J. Immunol.* **160**, 1552–1554.
- Gobel, T.W., and Dangy, J.P. (2000). Evidence for a stepwise evolution of the CD3 family. *J. Immunol.* **164**, 879–883.
- Kaufman, J. (2018). Unfinished business: evolution of the MHC and the adaptive immune system of jawed vertebrates. *Annu. Rev. Immunol.* **36**, 383–409.
- Kim, S.T., Touma, M., Takeuchi, K., Sun, Z.Y., Dave, V.P., Kappes, D.J., Wagner, G., and Reinherz, E.L. (2010). Distinctive CD3 heterodimeric ectodomain topologies maximize antigen-triggered activation of alpha beta T cell receptors. *J. Immunol.* **185**, 2951–2959.
- Kjer-Nielsen, L., Clements, C.S., Brooks, A.G., Purcell, A.W., McCluskey, J., and Rossjohn, J. (2002). The 1.5 Å crystal structure of a highly selected antiviral T cell receptor provides evidence for a structural basis of immunodominance. *Structure* **10**, 1521–1532.
- Koch, M., Camp, S., Collen, T., Avila, D., Salomonsen, J., Wallny, H.J., van Hateren, A., Hunt, L., Jacob, J.P., Johnston, F., et al. (2007). Structures of an MHC class I molecule from B21 chickens illustrate promiscuous peptide binding. *Immunity* **27**, 885–899.
- Kubota, T., Wang, J., Gobel, T.W., Hockett, R.D., Cooper, M.D., and Chen, C.H. (1999). Characterization of an avian (*Gallus gallus domesticus*) TCR alpha delta gene locus. *J. Immunol.* **163**, 3858–3866.
- La Gruta, N.L., Gras, S., Daley, S.R., Thomas, P.G., and Rossjohn, J. (2018). Understanding the drivers of MHC restriction of T cell receptors. *Nat. Rev. Immunol.* **18**, 467–478.
- Lahti, J.M., Chen, C.L., Sowder, J.T., Bucy, R.P., and Cooper, M.D. (1988). Characterization of the avian T cell receptor. *Immunol. Res.* **7**, 303–317.
- Li, X., Zhang, L., Liu, Y., Ma, L., Zhang, N., and Xia, C. (2020). Structures of the MHC-I molecule BF2*1501 disclose the preferred presentation of an H5N1 virus-derived epitope. *J. Biol. Chem.* **295**, 5292–5306.
- Li, Y., Yin, Y., and Mariuzza, R.A. (2013). Structural and biophysical insights into the role of CD4 and CD8 in T cell activation. *Front. Immunol.* **4**, 206.
- Parra, Z.E., and Miller, R.D. (2012). Comparative analysis of the chicken TCRalpha/delta locus. *Immunogenetics* **64**, 641–645.
- Reinherz, E.L., Tan, K.M., Tang, L., Kern, P., Liu, J.H., Xiong, Y., Hussey, R.E., Smolyar, A., Hare, B., Zhang, R.G., et al. (1999). The crystal structure of a T cell receptor in complex with peptide and MHC class II. *Science* **286**, 1913–1921.
- Rudolph, M.G., Stanfield, R.L., and Wilson, I.A. (2006). How TCRs bind MHCs, peptides, and coreceptors. *Annu. Rev. Immunol.* **24**, 419–466.
- Shigeta, A., Sato, M., Kawashima, T., Horiuchi, H., Matsuda, H., and Furusawa, S. (2004). Genomic organization of the chicken T-cell receptor beta chain D-J-C region. *J. Vet. Med. Sci.* **66**, 1509–1515.
- Sibener, L.V., Fernandes, R.A., Kolawole, E.M., Carbone, C.B., Liu, F., McAfee, D., Birnbaum, M.E., Yang, X., Su, L.F., Yu, W., et al. (2018). Isolation of a structural mechanism for uncoupling T cell receptor signaling from peptide-MHC binding. *Cell* **174**, 672–687 e627.
- Stewart-Jones, G.B.E., McMichael, A.J., Bell, J.I., Stuart, D.I., and Jones, E.Y. (2003). A structural basis for immunodominant human T cell receptor recognition. *Nat. Immunol.* **4**, 657–663.
- Taniuchi, I. (2018). CD4 helper and CD8 cytotoxic T cell differentiation. *Annu. Rev. Immunol.* **36**, 579–601.
- Tjoelker, L.W., Carlson, L.M., Lee, K., Lahti, J., McCormack, W.T., Leiden, J.M., Chen, C.L., Cooper, M.D., and Thompson, C.B. (1990). Evolutionary conservation of antigen recognition: the chicken T-cell receptor beta chain. *Proc. Natl. Acad. Sci. U. S. A.* **87**, 7856–7860.
- Tynan, F.E., Burrows, S.R., Buckle, A.M., Clements, C.S., Borg, N.A., Miles, J.J., Beddoe, T., Whisstock, J.C., Wilce, M.C., Silins, S.L., et al. (2005). T cell receptor recognition of a ‘super-bulged’ major histocompatibility complex class I-bound peptide. *Nat. Immunol.* **6**, 1114–1122.
- Wang, J.H. (2020). T cell receptors, mechanosensors, catch bonds and immunotherapy. *Prog. Biophys. Mol. Biol.* **153**, 23–27.
- Wang, J.H., and Reinherz, E.L. (2012). The structural basis of alphabeta T-lineage immune recognition: TCR docking topologies, mechanotransduction, and co-receptor function. *Immunol. Rev.* **250**, 102–119.
- Wu, Y., Wang, J., Fan, S., Chen, R., Liu, Y., Zhang, J., Yuan, H., Liang, R., Zhang, N., and Xia, C. (2017). Structural definition of duck major histocompatibility complex class I molecules that might explain efficient cytotoxic T lymphocyte immunity to influenza A virus. *J. Virol.* **91**, e02511–e02516.
- Zhang, L., Li, X., Ma, L., Zhang, B., Meng, G., and Xia, C. (2020a). A newly recognized pairing mechanism of the alpha- and beta-chains of the chicken peptide-MHC class II complex. *J. Immunol.* **204**, 1630–1640.
- Zhang, T., Liu, G., Wei, Z., Wang, Y., Kang, L., Jiang, Y., and Sun, Y. (2020b). Genomic organization of the chicken TCRbeta locus originated by duplication of a Vbeta segment combined with a trypsinogen gene. *Vet. Immunol. Immunopathol.* **219**, 109974.

iScience, Volume 23

Supplemental Information

**Structural and Biophysical Insights
into the TCR $\alpha\beta$ Complex in Chickens**

Lijie Zhang, Yanjie Liu, Geng Meng, Ruiying Liang, Bing Zhang, and Chun Xia

Supplemental items
Figures

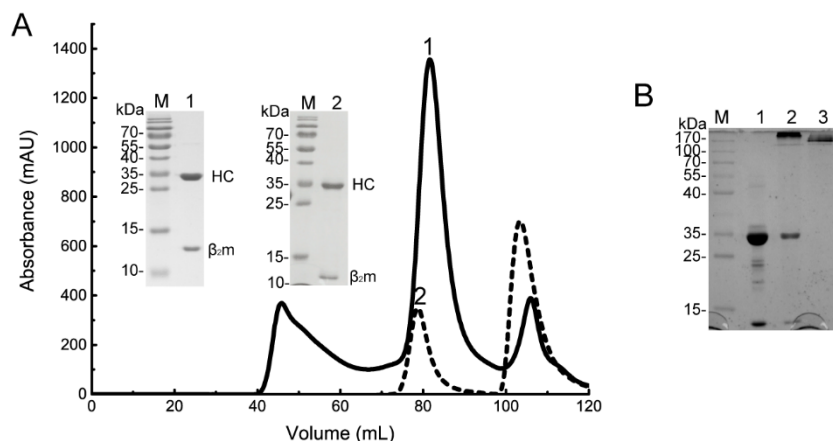


Figure S1. Production of the pBF2*1501 tetramer (Related to Figure 1). (A) The pBF2*1501-BSP complexes (solid line) were purified by chromatography on a Superdex 200 size-exclusion column and biotinylated using the BirA enzyme. The biotinylated pBF2*1501 complexes (dashed line) were subsequently purified using the same column. Peaks 1 and 2 represent the correctly refolded pBF2*1501-BSP complex and the biotinylated pBF2*1501 complex, respectively. The efficiency of purification of the complex was tested via SDS-PAGE. (B) Evaluation of tetramerization efficiency via SDS-PAGE. Lane 1 is untetramerized pBF2*1501 monomer, lane 2 is pBF2*1501 tetramer, and lane 3 is PE-labeled streptavidin.

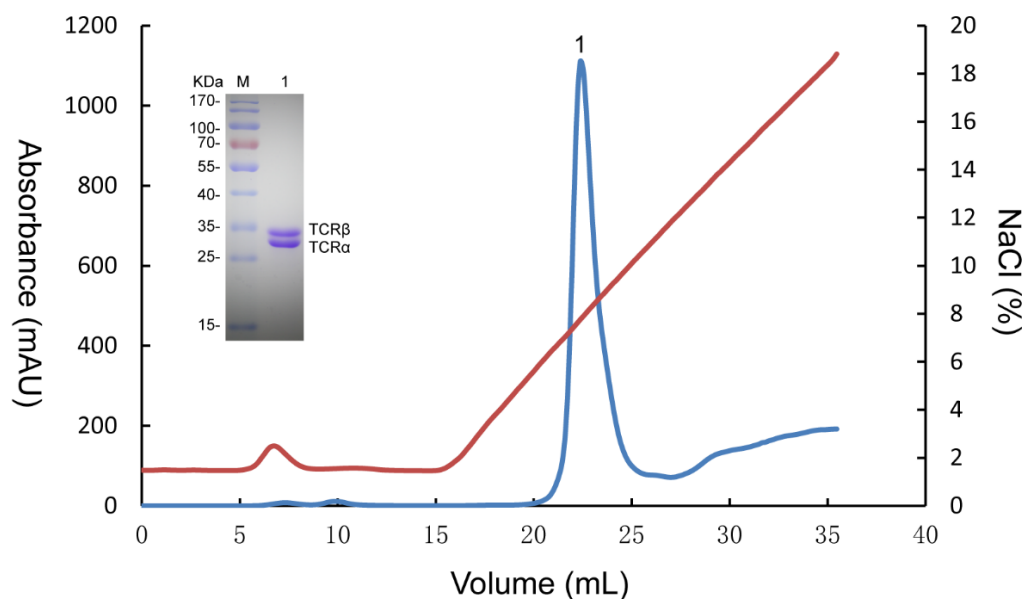


Figure S2. Assembly of the chicken TCR $\alpha\beta$ heterodimer (Related to Figure 2). Ch-TCR α and ch-TCR β chains were expressed and co-refolded *in vitro*. The ch-TCR $\alpha\beta$ heterodimer curve is shown in blue, and the NaCl concentration curve is shown in red. The insets show the SDS-PAGE (15%) analysis of the peak that is labeled on the curve. Lane M contains molecular mass markers (labeled in kDa).

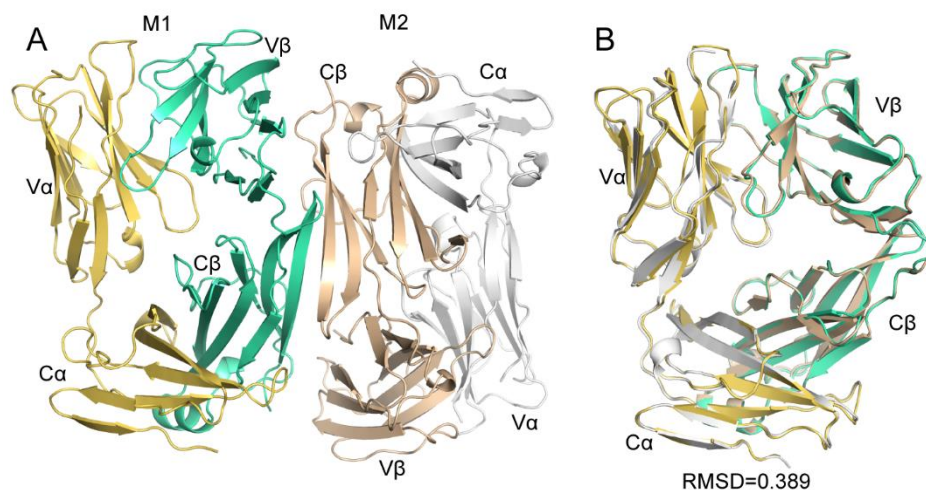


Figure S3. Overall structure of chicken TCR $\alpha\beta$ (Related to Figure 2). (A) Two molecules (M1 and M2) in an asymmetric unit are shown in cartoon representation. The ch-TCR $\alpha\beta$ molecules are packed “head to tail”. The α chain of the M1 molecule is shown in yellow-orange, the β chain of the M1 molecule is shown in cyan, and the α chain and the β chain of the M2 molecule are shown in light pink and in gray, respectively. (B) Superposition of M1 and M2. The structures of the M1 molecule were very similar to those of the M2 molecule, and the RMSD for all of the C α atoms in the two molecules was 0.3895.

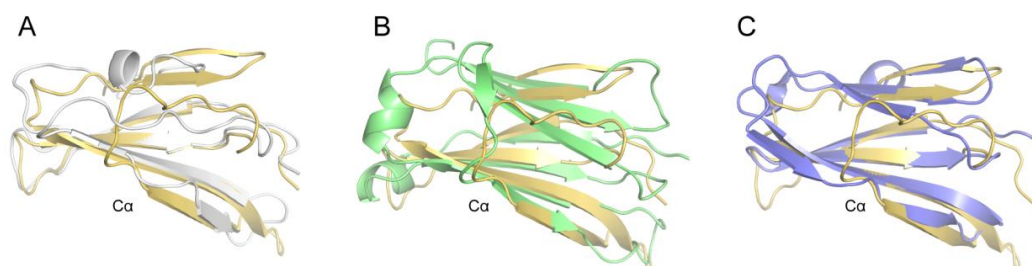


Figure S4. Connection between the ABED and CFG sheets of the C α domain of ch-TCR $\alpha\beta$ (Related to Figure 4). Superposition of the C α domain of ch-TCR $\alpha\beta$ and the C α domain of 2C-TCR $\alpha\beta$ (A) C domain of the antibody light chain (PDB: 1MLC) (B) and C γ domain of TCR $\gamma\delta$ (C). The C α domain of ch-TCR $\alpha\beta$ is shown in yellow-orange, the C domain of the antibody light chain is shown in gray, and the C γ domain of TCR $\gamma\delta$ is shown in slate.

Table S1. PCR primers specific for chicken TCR genes (Related to Figure 2).

Primers	Sequence (5'-3')
<i>Ch-TCRα</i> -cloning-forward primer	ATGGATTTTGTGAGTTTGCTTCTTGTTTTTC
<i>Ch-TCRα</i> -cloning-reverse primer	TCATTGATTTTTTTTCCACATAAG
<i>Ch-TCRβ</i> -cloning-forward primer	ATGTGGACAATTTGGTGCATGGTCTTG
<i>Ch-TCRβ</i> -cloning-reverse primer	CTAGTACATTTTCTTGTACCAAAGCATC
<i>Ch-TCRα</i> -expression-forward primer	CCGGAATTCATGCAGGTGCAGCAGGAGCCGTCG
<i>Ch-TCRα</i> -expression-reverse primer	CCGCTCGAGTTAGTTCAGGTTCTCATCTGTCTTG
<i>Ch-TCRβ</i> -expression-forward primer	CCGGAATTCATGGAGATTAACCAACCCTCAATTC
<i>Ch-TCRβ</i> -expression-reverse primer	CCGCTCGAGTTACTTCCCAGCTGTAGCACTTCTC
<i>Ch-TCRβ</i> (L141M) -forward primer	AGAAGAAGAAGGCCACAATGGTATGCCTGGCCTCTGGTTTC
<i>Ch-TCRβ</i> (L141M) -reverse primer	AACCAGAGGCCAGGCATACCAATTGTGGCCTTCTTCTTCTTG

Table S2. The RMSD values for main chain superposition of ch-TCR $\alpha\beta$ and other TCR $\alpha\beta$ molecules that have been resolved (Related to Figure 2).

number	PDB	Overall	α chain	α 1 domain	α 2 domain	β chain	β 1 domain	β 2 domain
1	1TCR	1.9559	1.8893	1.4080	2.1689	1.9175	0.7611	0.7754
2	3QH3	1.5960	1.8408	1.3602	2.4946	1.7031	0.7789	0.9415
3	2VLM	2.5061	1.8935	1.2091	2.5604	2.7177	0.9901	0.9922
4	3VXQ	2.0579	1.8767	1.4918	2.6762	1.8406	1.3183	0.8512
5	3VXT	2.2930	1.8406	1.3447	2.4408	2.4727	0.7940	0.9564
6	2NW2	1.8554	1.8741	1.3447	2.4060	1.7797	0.7732	0.9647
7	1KGC	2.0998	1.7001	1.5452	2.4575	2.0937	1.3099	0.9623
8	3SKN	2.1018	1.8008	1.3725	2.3780	2.1472	1.1740	1.1004
9	2BNU	2.3448	1.9808	1.1569	2.4623	2.4649	0.7616	0.9231
10	3DX9	2.4777	2.2047	1.5888	2.6606	2.3227	1.5093	0.9195
11	3UTP	2.3870	2.0550	1.3006	2.1924	2.2512	1.4052	1.0493
12	3QEU	2.0177	1.8309	1.4561	2.4347	2.0975	0.7782	0.9986
13	4JFH	2.2425	2.0359	1.3476	2.7692	2.3422	1.6909	0.9387
14	5NMD	2.2126	1.5539	1.1297	2.3246	2.5111	1.4310	0.8468
15	6AT6	2.0588	1.9343	1.4932	2.0293	1.9278	0.8368	1.0012
16	4GG8	2.5761	2.3022	1.6889	2.5064	2.2523	1.4854	1.0387
17	4E42	1.9533	2.0729	1.3151	2.5873	1.6488	1.3142	1.1269
18	2IAL	2.3207	1.6652	1.3925	2.5648	2.1434	0.8834	0.9980
19	4GKZ	2.2049	2.0421	1.5538	2.4580	2.1372	0.6114	0.9914
20	3QJF	1.8832	2.2017	1.3307	2.6464	1.6848	1.2135	1.0840
21	6CPH	1.9029	1.9978	1.6518	2.6505	1.5212	1.3788	0.9390
22	2Q86	1.6731	1.7162	1.0898	2.1142	1.6848	0.7379	0.9790
23	3AXL	2.2069	1.9374	1.0927	2.4578	2.1292	0.9373	1.0110
24	2EYS	2.4755	2.1096	1.2196	2.3824	2.3708	0.9767	0.9861
25	3TYF	1.7811	1.9347	1.34	2.1313	1.5448	1.0415	1.0140
26	4EI6	2.1232	1.7456	1.4341	2.3432	1.9363	1.2851	0.9904
27	4DZB	2.0890	2.1617	1.2290	2.2324	1.8788	1.4587	1.0056
28	4MNH	2.8916	2.1655	1.6232	2.4022	2.7404	1.9961	0.9140
29	4LFH	2.4674	2.0838	1.4420	2.3895	2.4516	1.8655	1.5204
30	1HXM	3.0576	2.7025	1.6079	2.6080	2.4617	1.5034	1.6092

Numbers 1 to 15 are TCR molecules associated with MHC-I molecules; numbers 16 to 21 are TCR molecules associated with MHC-II molecules; numbers 22 to 27 are innate-like TCR; and numbers 28 to 30 are TCR $\gamma\delta$.

Transparent Methods

Sorting epitope-specific CD8⁺ T-cells. According to the peptide-binding motif (X-R-X-X-X-X-Y) of the BF2*15:01 allele of B15-haplotype chickens, the peptide RREVHTYY (located at positions 123-130 of the PA protein, and named PA₁₂₃₋₁₃₀) was derived from the PA protein of the highly pathogenic avian influenza (HPAIV) H5N1 virus (Li et al., 2020; Wallny et al., 2006). PA₁₂₃₋₁₃₀ was synthesized and purified to 90% purity by reverse-phase high-performance liquid chromatography (HPLC) and mass spectrometry (SciLight Biotechnology LLC, Beijing, China). PE-labeled pBF2*15:01 tetramers for the detection of PA₁₂₃₋₁₃₀-specific CTL cells were constructed as previously reported (Li et al., 2020). Subsequently, according to our previously reported method, PA₁₂₃₋₁₃₀ peptide plus adjuvant was used to immunize B15 haplotype specific pathogen-free (SPF) chickens (BF2*15:01), and PA₁₂₃₋₁₃₀ peptide-specific T-cells were sorted (Li et al., 2020). A total of 8 seven-day-old B15 lineage SPF chickens were divided into two groups with 4 chickens in each group. One group was immunized with PA₁₂₃₋₁₃₀ plus adjuvant, and the other group was the control group. Each animal received a total of 3 immunizations at 7-day intervals. Seven days after the third immunization, peripheral blood lymphocytes (PBMC) were isolated from blood collected from the animals' wing veins, and 2×10^6 cells from each individual were stained with PE-labeled tetramers and an FITC-labeled mouse anti-chicken CD8 α monoclonal antibody (SouthernBiotech, USA). After staining, PA₁₂₃₋₁₃₀ peptide and CD8 double-positive T-cells were detected and sorted by flow cytometry (FACS Aria, BD, USA). The sorted cells were suspended in RPMI1640 medium containing 10% fetal bovine serum and counted again. More than 10^6 cell events could be used to extract mRNA.

Cloning *TCR α* and *TCR β* chains. Total RNA was extracted from the PA₁₂₃₋₁₃₀-specific CD8⁺ T-cells using TRIzol reagent, and RNA concentrations were measured via spectrophotometry. After confirmation of the integrity of the RNA by analysis on a 1.5% (w/v) agarose gel, it was reverse-transcribed into cDNA using the ExScript RT Reagent Kit (TaKaRa Biotechnology, China). Two pairs of primers were designed based on the sequences of the two known TCR genes (U-EF554736 and U-EF554782) and used to amplify full-length *TCR α* and *TCR β* sequences by the polymerase chain reaction (PCR) (Table S1). Amplifications were performed in a reaction volume of 50 μ l. The reaction contained 100-200 ng of cDNA, 25 pmol of each primer, 4 μ l of 2.5 mM dNTP, 10 \times PCR buffer with 15 mM MgCl₂, and 1 unit of HiFi DNA polymerase (Transgen Biotech, China). The thermal cycling conditions were as follows: initial denaturation at 98 $^{\circ}$ C for 5 min, followed by 32 cycles of 98 $^{\circ}$ C for 10 s, 60 $^{\circ}$ C for 15 s, and 72 $^{\circ}$ C for 1 min and final extension at 72 $^{\circ}$ C for 10 min. The PCR products were inserted into the pMD-18T vector (TaKaRa Biotechnology, China), and positive clones were selected and sent to BioSune (Shanghai, China) for sequencing. The sequences have been submitted to GenBank (National Center for Biotechnology Information: <https://www.ncbi.nlm.nih.gov/genbank/>) under the accession numbers GenBank: MN646854, MN646855.

Protein preparation. As described above, the *ch-TCR α* gene (encoding extracellular residues 1-218) and the *ch-TCR β* gene (encoding extracellular residues 1-238), with the addition of both *Eco*R I and *Xho* I sites, were cloned by PCR (Table S1). The PCR products were sequenced, ligated into the prokaryotic expression vector pET21a (Novagen) at the *Eco*RI and *Xho* I restriction sites, and transformed into *Escherichia coli* (*E. coli*) strain BL21 (DE3). Recombinant ch-TCR α and ch-TCR β were expressed in inclusion bodies and induced by 0.5 mM isopropyl β -D-thiogalactoside. To calculate the correct phase by the SAD method, site-directed mutagenesis was performed to construct the *ch-TCR β* chain containing the L141M mutation using overlap PCR with the Fast Mutagenesis System Kit (TransGen Biotech, China) (Table S1). The mutant *ch-TCR β* recombinant plasmid was then transformed into the methionine-auxotrophic *E. coli* strain B834 (DE3) for the expression of SeMet-substituted ch-TCR β proteins (SeMet-ch-TCR β). SeMet-ch-TCR β was prepared as previously described (Chen et al., 2018; Hendrickson et al., 1990).

Assembly of antigen-specific ch-TCR $\alpha\beta$ heterodimers. For *in vitro* refolding, purified ch-TCR α and SeMet-ch-TCR β inclusion bodies were diluted at a ratio of 1:2 in a refolding solution containing 100 mM Tris-HCl, 5 M guanidinium chloride, 40 mM L-arginine-HCl, 2 mM EDTA, 5 mM reduced glutathione and 0.5 mM oxidized glutathione, pH 8.0. After stirring for 1 hour at 4 $^{\circ}$ C, the refolding solution was dialyzed to eliminate the Gua-HCl. The folding solution was concentrated and purified by Resource Q anion-exchange chromatography (GE Healthcare, China) as previously described (Chen et al., 2017). Ch-TCR α and ch-TCR β were refolded and purified as described above for ch-TCR α and SeMet-ch-TCR β .

Crystallization and data collection. Purified SeMet-ch-TCR $\alpha\beta$ and ch-TCR $\alpha\beta$ heterodimers were

concentrated to 4 mg/mL and 8 mg/mL, respectively, in a buffer containing 20 mM Tris-HCl (pH 8.0) and 50 mM NaCl for crystallization. After mixing with the reservoir buffer at a 1:1 ratio, the concentrated ch-TCR $\alpha\beta$ heterodimers were crystallized by the sitting-drop vapor diffusion method at 18 °C. Index, Crystal Screen I/II, and Crystal Screen Cryo I/II Kits (Hampton Research, Riverside, CA) were used to screen for optimal crystal growth conditions. After 7 days, SeMet-ch-TCR $\alpha\beta$ crystals were obtained with solution No. 22 from the PEG/Ion 2 Kit (0.2 M tribasic ammonium citrate pH 7.0, 20% w/v polyethylene glycol 3350) (Hampton Research), and ch-TCR $\alpha\beta$ crystals were obtained with solution No. 45 from the PEG/Ion Kit (0.2 M tribasic lithium citrate tetrahydrate, 20% PEG3350) (Hampton Research). The preliminary screening conditions were further optimized manually using graded variations in the concentrations of precipitant and salt in hanging drop vapor diffusion experiments at 4 °C and 18 °C. SeMet-ch-TCR $\alpha\beta$ crystals and ch-TCR $\alpha\beta$ crystals were obtained under optimized conditions at 18 °C (0.22 M tribasic ammonium citrate pH 7.0 with 18% w/v polyethylene glycol 3350 and 0.25 M tribasic lithium citrate tetrahydrate with 24% PEG 3350, respectively). Prior to data collection, all crystals were cryoprotected in reservoir buffer containing 30% (v/v) glycerol and flash-cooled at 100 K. The 1.9 Å diffraction data of the SeMet-ch-TCR $\alpha\beta$ crystal and the 2.1 Å diffraction data of the ch-TCR $\alpha\beta$ crystal were collected at 100 K. Data collection was performed at the Shanghai Synchrotron Radiation Facility using beamline BL17U at 0.97923 Å with an ADSC 315 CCD detector (Shanghai, China) (Wang et al., 2016). The collected intensities were indexed, integrated, corrected for absorption, scaled, and merged using the HKL3000 package (Minor et al., 2006).

Structure determination and refinement. The data collection and refinement statistics are summarized in Table 1. Structural determination was performed using the SAD method with selenomethionine as an anomalous signal as previously reported (Liu et al., 2012). Briefly, the expected heavy atoms were determined by SHELXD (Schneider and Sheldrick, 2002), and the initial phases were then determined using Phaser (McCoy, 2007). Density modification was performed by DM (Cowtan and Main, 1996). Approximately 90% of the ch-TCR $\alpha\beta$ residues were traced automatically by ARP/Warp (Perrakis et al., 2001). The structure of ch-TCR $\alpha\beta$ was solved by molecular replacement with Phaser in the CCP4 package and SeMet-ch-TCR as the search model (Collaborative Computational Project, 1994). Extensive model building and restrained refinement were performed with COOT (Emsley and Cowtan, 2004) and REFMAC5 (Murshudov et al., 1997), respectively. Refinement cycles were performed using the phenix.refine program in the PHENIX package (Adams et al., 2002) with isotropic ADP refinement and bulk solvent modeling. The stereochemical quality of the final models was validated using the PROCHECK program (Laskowski et al., 1993).

Data analysis. The SignalP 3.0 Server was used to predict the presence and location of signal peptide cleavage sites (Almagro Armenteros et al., 2019). Structural illustrations were generated using PyMOL (<http://www.pymol.org/>) and UCSF Chimera (<http://www.cgl.ucsf.edu/chimera/>). The isotropic B factor was calculated using the equation $B=8\pi^2\langle\mu^2\rangle$. Solvent-accessible surface areas were calculated using the PDBePISA webpage (<http://www.ebi.ac.uk/pdbe/pisa/picite.html>). Protein amino acid sequences were compared using Clustal Omega (<http://www.ebi.ac.uk/Tools/msa/clustalo/>) (Chojnacki et al., 2017). The coordinates and structure factors generated in this study have been submitted to the Protein Data Bank (<https://deposit-pdbj.wwpdb.org/deposition/>) under accession number 6LIR.

Supplemental References

- Adams, P.D., Grosse-Kunstleve, R.W., Hung, L.W., Ioerger, T.R., McCoy, A.J., Moriarty, N.W., Read, R.J., Sacchettini, J.C., Sauter, N.K., and Terwilliger, T.C. (2002). PHENIX: building new software for automated crystallographic structure determination. *Acta Crystallogr D Biol Crystallogr* *58*, 1948-1954.
- Almagro Armenteros, J.J., Tsirigos, K.D., Sonderby, C.K., Petersen, T.N., Winther, O., Brunak, S., von Heijne, G., and Nielsen, H. (2019). SignalP 5.0 improves signal peptide predictions using deep neural networks. *Nat Biotechnol* *37*, 420-423.
- Chen, R., Zhang, L., Qi, J., Zhang, N., Zhang, L., Yao, S., Wu, Y., Jiang, B., Wang, Z., Yuan, H., *et al.* (2018). Discovery and Analysis of Invertebrate IgVJ-C2 Structure from Amphioxus Provides Insight into the Evolution of the Ig Superfamily. *Journal of immunology* *200*, 2869-2881.
- Chen, Z., Zhang, N., Qi, J., Chen, R., Dijkstra, J.M., Li, X., Wang, Z., Wang, J., Wu, Y., and Xia, C. (2017). The Structure of the MHC Class I Molecule of Bony Fishes Provides Insights into the Conserved Nature of the Antigen-Presenting System. *Journal of immunology* *199*, 3668-3678.
- Chojnacki, S., Cowley, A., Lee, J., Foix, A., and Lopez, R. (2017). Programmatic access to bioinformatics tools from EMBL-EBI update: 2017. *Nucleic Acids Res* *45*, W550-W553.
- Collaborative Computational Project, N. (1994). The CCP4 suite: programs for protein crystallography. *Acta Crystallogr D Biol Crystallogr* *50*, 760-763.
- Cowtan, K.D., and Main, P. (1996). Phase combination and cross validation in iterated density-modification calculations. *Acta Crystallogr D Biol Crystallogr* *52*, 43-48.
- Emsley, P., and Cowtan, K. (2004). Coot: model-building tools for molecular graphics. *Acta Crystallogr D Biol Crystallogr* *60*, 2126-2132.
- Hendrickson, W.A., Horton, J.R., and LeMaster, D.M. (1990). Selenomethionyl proteins produced for analysis by multiwavelength anomalous diffraction (MAD): a vehicle for direct determination of three-dimensional structure. *The EMBO journal* *9*, 1665-1672.
- Laskowski, R.A., Moss, D.S., and Thornton, J.M. (1993). Main-chain bond lengths and bond angles in protein structures. *J Mol Biol* *231*, 1049-1067.
- Li, X., Zhang, L., Liu, Y., Ma, L., Zhang, N., and Xia, C. (2020). Structures of the MHC-I molecule BF2*1501 disclose the preferred presentation of an H5N1 virus-derived epitope. *J Biol Chem* *295*, 5292-5306.
- Liu, J., Qian, X., Chen, Z., Xu, X., Gao, F., Zhang, S., Zhang, R., Qi, J., Gao, G.F., and Yan, J. (2012). Crystal structure of cell adhesion molecule nectin-2/CD112 and its binding to immune receptor DNAM-1/CD226. *Journal of immunology* *188*, 5511-5520.
- McCoy, A.J. (2007). Solving structures of protein complexes by molecular replacement with Phaser. *Acta Crystallogr D Biol Crystallogr* *63*, 32-41.
- Minor, W., Cymborowski, M., Otwinowski, Z., and Chruszcz, M. (2006). HKL-3000: the integration of data reduction and structure solution--from diffraction images to an initial model in minutes. *Acta Crystallogr D Biol Crystallogr* *62*, 859-866.
- Murshudov, G.N., Vagin, A.A., and Dodson, E.J. (1997). Refinement of macromolecular structures by the maximum-likelihood method. *Acta Crystallogr D Biol Crystallogr* *53*, 240-255.
- Perrakis, A., Harkiolaki, M., Wilson, K.S., and Lamzin, V.S. (2001). ARP/wARP and molecular replacement. *Acta Crystallogr D Biol Crystallogr* *57*, 1445-1450.
- Schneider, T.R., and Sheldrick, G.M. (2002). Substructure solution with SHELXD. *Acta Crystallogr D Biol Crystallogr* *58*, 1772-1779.
- Wallny, H.J., Avila, D., Hunt, L.G., Powell, T.J., Riegert, P., Salomonsen, J., Skjodt, K., Vainio, O., Vilbois, F., Wiles, M.V., *et al.* (2006). Peptide motifs of the single dominantly expressed class I molecule explain the striking MHC-determined response to Rous sarcoma virus in chickens. *Proceedings of the National Academy of Sciences of the United States of America* *103*, 1434-1439.
- Wang, Z., Pan, Q., Yang, L., Zhou, H., Xu, C., Yu, F., Wang, Q., Huang, S., and He, J. (2016). Automatic crystal centring procedure at the SSRF macromolecular crystallography beamline. *J Synchrotron Radiat* *23*, 1323-1332.